Journal of Renewable Materials

Tech Science Press

Characterization of Manmade and Recycled Cellulosic Fibers for Their Application in Building Materials

Nadezda Stevulova[1,*], Viola Hospodarova[1], Adriana Estokova[1], Eva Singovszka[1], Marian Holub[1], Stefan Demcak[1], Jaroslav Briancin[2], Anton Geffert[3], Frantisek Kacik[3], Vojtech Vaclavik[4] and Tomas Dvorsky[4]

[1]Technical University of Kosice, Faculty of Civil Engineering, Institute of Environmental Engineering, Vysokoskolska 4, 04200 Kosice, Slovakia.

[2]Institute of Geotechnics of the Slovak Academy of Sciences, Watsonova 45, 043 53 Kosice, Slovakia.

[3]Technical University in Zvolen, Faculty of Wood Sciences and Technology, Department of Chemistry and Chemical Technologies, T. G. Masaryka 2117/24, 960 53 Zvolen, Slovakia.

[4]VSB-Technical University of Ostrava, Faculty of Mining and Geology, Department of Environmental Engineering, 17. listopadu 15/2172, 708 33 Ostrava-Poruba, Czech Republic.

[*]Corresponding Author: Nadezda Stevulova. Email: nadezda.stevulova@tuke.sk.

Abstract: The aim of this study was to characterize two types of cellulosic fibers obtained from bleached wood pulp and unbleached recycled waste paper with different cellulose content (from 47.4 percent up to 82 percent), to compare and to analyze the potential use of the recycled fibers for building application, such as plastering mortar. Changes in the chemical composition, cellulose crystallinity and degree of polymerization of the fibers were found. The recycled fibers of lower quality showed heterogeneity in the fiber sizes (width and length), and they had greater surface roughness in comparison to high purity wood pulp samples. The high purity fibers (cellulose content > 80.0 percent) had greater crystallinity and more homogeneous and smooth surfaces than the recycled fibers. The presence of calcite and kaolinite in all of the recycled cellulosic fibers samples was confirmed, whereas only one wood pulp sample contained calcite. The influence of the chemical composition was reflected in the fiber density values. Changes in the chemical composition and cellulose structure of the fibers affected the specific surface area, porosity and thermo physical properties of the fibers. More favorable values of thermal conductivity were reached for the recycled fibers than for the wood pulp samples. Testing the suitability of the recycled fibers with inorganic impurities originating from the paper-making processes for their use as fillers in plastering mortars (0.5 wt.% fiber content of the total weight of the filler and binder) confirmed their application by achieving a compressive strength value of 28 day-cured fiber-cement mortar required by the standard as well as by measured more favorable value of capillary water absorption coefficient.

Keywords: Wood pulp; waste paper; fiber properties characterization; compressive strength of mortars

1 Introduction

There is general public awareness of the exhaustion of nonrenewable sources of raw materials, much of which has been caused by industrial and agricultural production that is connected to extensive pollution of all the components of the environment, thus causing climatic changes; as a result, there is an enhanced demand for sustainable products based on renewable sources [1]. The construction sector is one of the pillars in the economy of the society that negatively affects the surrounding environment with pollutants

due to high consumption of raw materials and energy resources. The actual key issue in forming a sustainable building industry is to minimize the excavation of natural resources, to reduce the effect of human activities on the people's health and the environment, and to replace petroleum and other non-biodegradable based products with bio-based materials from renewable resources [2]. Therefore, sustainable building structures play an important role in the reduction of material and energy costs, and contribute to healthy living in building by reducing negative environmental impacts. The focus on the sustainable use of natural and biodegradable resources in civil engineering involves the reuse of recyclable construction materials after the demolition of buildings but mainly to utilize environmentally compatible raw and secondary materials related to manufacturing environmental friendly materials/products [3]. The development of sustainable building materials is increasingly linked to the use of raw materials from fast-renewable sources represented by biomass. The utilization of this attractive organic material in building materials preparing allows on the one hand reducing the load on the environment [4], and on the other hand assists the development of societies centered upon bio-based economies, which are characterized by both reduced dependence upon imported fossil fuels or mineral resources and reduced greenhouse gases emissions [5].

The use of green materials in the building industry as a major strategic approach of this century is mainly focused on the development bio-based building materials [6]. In this context, cellulosic fibers obtained from biomass are attractive because of their advantageous properties and environmental benefit [7]. They are readily available, environmental friendly, and technologically suitable; therefore, they are an excellent raw material for the future application. This fibrous substance as a nonhazardous and relatively low cost material offers the potential of a zero carbon footprint, biodegradability, renewability, and recyclability [8], and it is being intensively investigated for the potential to be applied as a filler and reinforcement in biomass-based cement composites [9]. Plant fibers, in regard to their implementation in building materials are classified as non-wood and wood fibers [10]. Non-wood cellulosic fibers are mainly derived from agricultural plants. Wood pulp in the form of cellulosic fibers is the main product from wood-biomass processing [11]. Currently, research has been concentrated on the utilization of non-wood agricultural waste for many applications in comparison to woody biomass [12].

In addition to the above mentioned advantages of cellulosic fibers, this material has a number of fascinating mechanical (acceptable specific strength) and physical properties (low density approximately 1.5 g/cm^3; low thermal conductivity ~ 0.3 W/m.K in the longitudinal direction; ~ 0.2 W/m.K in the transverse direction) [7,13]. Their mechanical properties depend on their physical, chemical and morphological characteristics such as chemical composition, crystal structure, fiber orientation, diameter/cross-sectional area of the fiber and average chain length of the cellulose polymer. Natural fibers are comprised of microfibrils of cellulose in a matrix of hemicellulose and lignin. As generally known, this type of structure and its chemical composition is responsible for its mechanical properties. Because hydrogen bonds between the long chains are in the natural fibers, they have the necessary stiffness and strength. However, microfibril angles as structural parameters of wood cells have an important influence on their mechanical properties. The smaller the microfibrils angle, the higher the longitudinal Young´s modulus of the wood cell [14].

The strength of the fiber varies with its diameter and length and depends on fiber origin. This is probably the reason why the mechanical properties of the different fiber types cover relatively wide range [15]. It has been found that industrially pulped hardwood fibers have a higher stiffness (approximately 40 GPa) than their corresponding soft wood fibers (14-27 GPa) [16]. The tensile strength of wood fibers is in the range of 1000-1200 MPa.

As it was found [17], the matrix cracks initiated during tensile-stress response test of sisal fiber reinforced composite are bridged by the longitudinal fibers.

All of these aforementioned properties are potential advantages that make cellulose fibers convenient materials for fiber-cement application. The natural-fiber cement composites are mainly applied in non-

structural thin-walled materials, mainly thin-sheet products for partitions, building envelopes or flat sheets for ceilings, roofing tiles and pre-manufactured components in general [18].

However, some issues of cellulosic fibers, such as their hydrophilic nature, low resistance against fire, degradation of fibers in the cement matrix, tendency for forming fiber clumps, and low compatibility between both the inorganic and organic phases are negative attributes for their application in building products [19]. Production of commercial cellulosic fibers (CFs) with low degree of water absorbency is costly. Therefore there are efforts to find a cheaper replacement for CFs. One of alternatives is to use the waste paper as a possible and valuable resource of CFs in cement-based materials. Waste paper recycling offers an economic benefit associated with the reduction of the risks of environmental impact of the primary produced CFs by chemical pulping. This trend of the incorporation of recycled CFs in cement-based composites is at the centre of current attention [20]. To develop cement composites/mortars based on recycled CFs providing thermal comfort inside buildings, it requires a complex characterization of their properties (chemical and phase composition, degree of crystallinity, morphology, and thermal conductivity and stability) by using adequate methods. The purpose of this study was to assess and compare morphology, dimensions, thermal conductivity, chemical composition, structure, and the thermal behavior of two kinds of cellulosic fibers (bleached wood pulp and recycled waste paper). To confirm their suitability for use as filler in plastering mortars, the compressive strength of 28-day-cured fiber-cement samples was tested.

2 Materials and Methods

2.1 Materials

Two kinds of cellulosic fibers, from wood processing (mainly the sulfate beech tree cellulose) and recycling wastepaper, were used. Six cellulosic fibers samples were provided by the company Greencel Ltd. (Hencovce, Slovakia). As shown in Fig. 1, these samples are visually different in color. Samples 1-3 represent white wood pulps (WPs) and samples 4-6 correspond to gray recycled cellulosic fibers (RCFs).

Figure 1: Greencel cellulosic fibers: wood pulp (a) and recycled wastepaper fibers (b)

2.2 Methods of Fiber Characterization

The physical and chemical properties of fibers after they were dried in a muffle furnace (Labotherm L5/11/B180; Nabertherm GmbH, Lilienthal, Germany) at a temperature of 80°C to a constant weight (24 hours) were characterized by sophisticated methods.

2.2.1 Density

This elementary physical property of cellulosic fibers was determined by a pycnometric method. A glass pycnometer flask NS 10/19 (Paul Marienfeld GmbH & Co.KG, Lauda-Königshofen, Germany) with a 25 ml volume and a close-fitting ground glass stopper with a capillary hole through it was used. Hexane (655 kg/m^3) was used as the working liquid. The measurement was carried out under laboratory

conditions at a temperature of 23 ± 1°C. The density of cellulosic fibers was calculated as the weight difference of a pycnometer with and without a fiber sample. The sample density is the average of three measurements.

2.2.2 Bulk Density

The bulk density of cellulosic fibers as the ratio of the mass of an untapped powdered sample and its volume (including the voids between fibers) was determined by using the tester EV-02 (Electrolab, Mumbai, India). The fiber sample was poured through a funnel into a measuring cup of 25 cm^3. By weighing the empty cup and a subsequently fiber-filled cup, the bulk density was calculated. For the determination of this property, we repeated the measurement of each sample three times in order to reach a good accuracy (< 5%).

2.2.3 Dimensions Characterization of Fibers

Average fiber length (L) and width (D) as well as aspect ratio (L/D) of the WP and RCF samples were determined by an image analysis method on the L&W Fiber Tester (ABB AB/Lorentzen & Wettre, Kista, Sweden). L&W Fiber Tester is an instrument for advanced analysis of fiber dimensions and fiber length distributions. It is fully automated and comes with a carousel with 6 glass beakers. The apparatus is a type of two-dimensional imaging technology. For fiber dimensions measurement, a fiber suspension containing 1 g of fibers in 1 liter of suspension is prepared. Approximately 300 ml of this suspension is placed in a beaker and then it is placed on the carousel. The fiber suspension is sucked in the measurement area. The fibers are oriented in a plane between two glass plates with 90^o angle relative to the illumination/camera axis. A very small measurement gap between plates (0.5 mm) secures a good alignment of the fibers. The entire fiber can then be seen and detected by the camera. True fiber length instead of projected fiber length and fiber deformations is measured. The fiber length distribution is in 75 classes that are divided by 0.1 mm, and they are in the measuring range from 0.01 to 7.5 mm. The fiber width distribution is in 50 classes that are divided by 2 μm, and they are in the measuring range from 10 to 100 μm. The test is completed after a measurement time of 150 seconds, which corresponds to the measurement of the necessary number of fibers (20,000). Resolution within measurement range is 0.1 μm. Repeatability is as follows: length 1.5%, width 1%. A cleaning system with automatic separation of the plates keeps the passage free. The test of each fiber sample was performed in triplicate. A histogram showing the fiber lengths distribution into six fractions for each investigated cellulosic sample is presented in 3.2.2.

2.2.4 Specific Surface Area and Porosity

The principle of specific surface area measurement is based on the well-known theory developed by Brunauer, Emmett and Teller (B.E.T. theory) for multilayer gas molecules adsorption on the evacuated surface of the solid particles. For comparison, Langmuir theory was also used. Low-temperature nitrogen molecules adsorption isotherms were experimentally measured at 77 K using a Quantachrome Nova 1000e (Quantachrome GmbH & Co. KG, Odelzhausen, Germany). The sample's surface area is calculated as the product of the number of adsorbed molecules in a monolayer covering the fiber surface and the cross-sectional area of an adsorbate molecule. Experimental isotherms of adsorbed gas volumes at equilibrium gas pressures allow for the computation of pore sizes distributions. The classical HK (Horvath-Kawazoe), DR (Dubinin-Radushkevich), SF (Saito-Foley) modes and the more accurate NLDFT (non-local density functional theory) were used to analyze the total micropore volume and micropore radius.

2.2.5 Heat Transfer Characteristics

The heat transfer characteristics such as thermal conductivity, volume heat capacity and thermal diffusivity of cellulosic fibrous samples were measured by the commercial device ISOMET 2114 (Applied Precision, Bratislava, Slovakia) with a noodle probe. The course of the time dependence of the

thermal response to the pulses of heat flux created by scattered electric power in a probe resistor in the analyzed material was recorded. The measured temperature is directly evaluated as a function of time by means of polynomial regression. The value of the coefficient of thermal conductivity is calculated from the coefficients determined by this regression.

2.2.6 Surface Morphology and Elemental Chemical Composition

A MIRA 3 FE Scanning electron microscopy (SEM) (TESCAN Ltd., Brno, Czech Republic) with a Schottky emitter for high-resolution was used to observe the surface morphological changes of the samples. Fiber samples were glued on carbon- adhesive films coated with a gold layer by using a vacuum-sputter coater to avoid charging under the electron beam. The accelerating voltage of SEM was 10 kV; the magnification was 1500×. The determination of the elemental chemical composition of samples was performed by an energy-dispersive X-ray unit (EDX).

2.2.7 Chemical Composition

The chemical composition of the main cellulosic and non-cellulosic components of WPs and RCFs samples was analyzed. The analytical methods for determining of the total content of polysaccharides and the contents of cellulose, hemicelluloses, acid-insoluble (Klason) lignin, extractives, and ash have been described in detail in a previous work [21]. The moisture content was determined by a gravimetric method from the difference in weight of the samples before and after drying. The drying of the fiber samples to an absolute dry condition was done in a laboratory drying oven (Ecocell 22, BMT Medical Technology, Brno, Czech Republic) at 103 ± 2°C. Mass measurements were made with precision to the level of 0.0001 g.

2.2.8 Molecular Mass Distribution

The molar mass distribution analysis of the cellulose in the WP and RCF samples was determined by size exclusion chromatography (SEC) after their conversion into tricarbanilates. This method is described in detail in previous works [21,22]. Data acquisitions were carried out with the ChemStation software (Agilent Technologies, Santa Clara, USA) and calculations were performed with the Clarity GPC (Gel Permeation Chromatography) module (DataApex, Prague, Czech Republic). The numerical outputs obtained for Mn (number-average molecular mass) and Mw (weight-average molecular mass) were recalculated to underivatized cellulose by multiplication with the coefficient k = 162/519. The polydispersity index (PDI) of cellulose was calculated as the ratio Mw/Mn. The degree of polymerization (DP) values were calculated by dividing the molar mass by the monomer equivalent weight of anhydroglucose (DPw = M/162).

2.2.9 Phase Analysis

The presence of crystalline and/or amorphous phases in the samples was analyzed using a Bruker D2 Phaser X-ray powder diffractometer (Bruker AXS GmbH, Karlsruhe, Germany) in Bragg-Brentano geometry. The relative amount of crystalline cellulose as crystallinity index (CrI) and crystallite size of crystalline cellulose in six different samples were established. The diffraction patterns produced using CuKα radiation (λ = 0.154060 nm) with Ni Kβ filters, and a scintillation detector at a voltage of 30 kV and a current of 10 mA were recorded in the range of 2θ from 5° to 50°. The scan conditions include a recording time of 6.5 hours and a step size of 0.02° (2θ), counting by 10 seconds per step. The XRD patterns were processed by using the software Diffrac. EVA v. 2.1. The ICDD-PDF2 database (ICDD, Philadelphia, USA) containing approximately 300,000 entries was utilized for the phase identification. In this study, the crystallinity index of cellulose CrI (Eq. (1)), such as the relative degree of crystallinity, was calculated from the XRD patterns of the fibrous samples by using the Segal peak height method [23].

$$CrI = \frac{I_{200} - I_{AM}}{I_{200}} \times 100\% \quad (1)$$

where I_{200} is the maximum intensity of the diffraction (200) peak at a 2θ angle ranging between 22°-23°, which represents both crystalline and amorphous cellulose. I_{AM} is the intensity of the diffraction peak of the amorphous material. It is taken at a 2θ angle between 18° and 19°, where a minimum intensity is observable [24]. The apparent crystallite sizes (L) of the Greencel cellulosic fibers in the (200) planes were calculated by using Scherrer's formula (2) [25] as follows:

$$L = \frac{K \times \lambda}{(\beta \times \cos\theta)} \quad (2)$$

where K is a dimensionless correction factor (0.94) called Scherrer's constant, λ is the wavelength of the X-ray beam (0.15406 nm), β is the width of the peak at the half maximum height of the diffraction peak [radians] and θ is the Bragg angle corresponding to the (200) plane.

2.2.10 Chemical Functional Groups Identification

The identification of the different chemical groups that constitute the WP and RCF samples was performed from the Fourier-transform infrared spectra measured on an Alpha Bruker Platinum-ATR (Bruker Optic GmbH, Ettlingen, Germany) spectrometer within the wave number range of 4000-400 cm^{-1} at a resolution of 4 cm^{-1}. A total of 24 scans were taken for each sample. Avicel microcrystalline cellulose (Sigma-Aldrich, Saint-Louis, USA) was used as a reference cellulosic material of high purity for a correct identification of function groups in FTIR spectra of WP and RCF samples.

2.2.11 Thermal Behavior

The thermo gravimetric (TG) analysis and differential scanning calorimetric (DSC) method were carried out by using an STA 449F3 Jupiter instrument (Netzsch, Selb, Germany). The record of mass loss of each sample in response to an ambient temperature of up to 1000°C was collected to determine both the TG and derivative thermo gravimetric (DTG) curves. Approximately 8 ± 1 mg of the sample was uniformly placed into the alumina crucible of the thermal analyzer, and the thermal decomposition of the samples was monitored at atmospheric pressure in the presence of high-purity nitrogen with a flow rate of 100 mL/min at a constant heating rate of 10 °C/min.

2.3 Preparation of Mortar Specimens and Testing Methods

The application potential in making cement-plastering mortars of low quality cellulosic fibers originating from waste paper in comparison to the bleached wood pulp with high cellulose content was evaluated by the mechanical properties of the mortar bodies after 28 days of curing. Mortar mixtures consisted of the Ordinary Portland cement CEM I 42.5 N (Povazska Cement Factory Ltd., Ladce, Slovakia), standard natural silica sand (Filtracni pisky Ltd, Chlum, Czech Republic), WP and RCF addition and water. Mortar mixtures with 0.5 wt.% WP and RCF addition related to the total weight of the filler and binder were prepared. The composition of fiber-cement mixture was based on STN EN 196-1 [26] and the water/cement ratio (w/c) was 0.55.

The preparation of mortars started with soaking of dry fibers and manual mixing in approximately 50 wt.% of water. The remaining water, the required amount of sand, and the cement were mixed by mechanical stirring in a laboratory mixer BS MI-CM5AX (BETON SYSTEM Ltd, Brno, Czech Republic) in accordance with standard [37] (to ensure the homogenous distribution of fibers in a cement mixture) at a low speed for 5.5 min. Filling the moulds (40 × 40 × 160 mm) with fresh fiber-cement mixture took place in two layers, and each layer was optimally compacted on a flow table by upsetting with 60 impacts [26]. The compaction process ensures the relative movement of all the components of the mixture so as to group as closely as possible and form a compact mass without air gaps. The filled molds were covered with a PVC foil to prevent the water from evaporating from the fresh mixture as it is needed to hydrate the cement. Two days after filling, the specimens were demolded and placed in a water bath.

The strength tests of 28-day-cured fiber-cement mortars were carried out by using a compression test machine (FORM+TEST Seidner & Co. GmbH, Germany) according to standard [27]. In the compressive strength testing, the loading rate was 2400 ± 200 N/s, while the three-point bending test was performed at a loading rate 50 ± 10 N/s. To determine the mechanical average values of the fiber-cement mortar, a series of three prisms with and without fibers was fabricated.

The capillary water absorption coefficient of two selected 28-day-cured fiber-cement mortars based on fiber samples 2 and 5 representing corresponding fiber group was determined according to standard procedure [28]. Sealing compound-paraffin wax was applied to the longitudinal sides of the test specimens and they were broken into two halves. The bodies thus prepared were inserted downwards into a water vessel having a water level of 5-10 mm. To ensure complete contact with water, washers were placed between the bottom of the vessel and the test body (its fractured surface). A constant water level was maintained throughout the test. The capillary water absorption coefficient (C) [$kg/m^2min^{0.5}$] was determined from the difference of the two measured values after 10 and 90 minutes, respectively, according to the Eq. (3)

$$C = 0.1 \times (M2 - M1) \quad (3)$$

where M1 and M2 is the sample mass after 10 and 90 minutes, respectively. The resulting average capillary water absorption coefficient value is given with an accuracy of 0.03 $kg/m^2min^{0.5}$.

3 Results and Discussion

3.1 Chemical Composition

Tab. 1 shows the chemical composition of the studied cellulosic fiber samples. As shown, two sets of cellulosic fiber samples (WP and RCF) differ in the content of a main component (hollocellulose). The first high purity set of samples (1-3) is characterized by a high holocellulose content > 99 percent, whereas the samples of the second set (4-6) have a lower holocellulose content by 18-29 percent. A relatively large difference in the cellulose content in the samples is also observed. The cellulose portion in the WP samples (1 and 2) is approximately 81-82 percent, but this substance is represented by only 47-62 percent of the WP sample (3) and RCF (samples 4-6). The amount of hemicelluloses in the samples ranges from 17-37 percent; the highest content is in sample 3. Four samples (samples 3-6) have a cellulose/hemicellulose ratio ranging between 1.7 to 2.3 what is similar to nanocellulose samples with typical ratios between 1 and 2.2 [29]. As expected, the cellulose/hemicellulose ratio was relatively high (4.2-4.8) in the two WP samples (1 and 2).

Table 1: Chemical composition of WP (1-3) and RC (4-6) fiber samples

Components of cellulosic fibers (%)	Component content (%) in cellulosic fibers samples					
	1	2	3	4	5	6
Holocellulose	99.11 ± 1.9	99.67 ± 1.6	99.09 ± 2.1	71.03 ± 2.1	71.98 ± 1.3	81.30 ± 2.2
Cellulose	81.99 ± 2.1	80.49 ± 1.7	62.13 ± 3.2	47.40 ± 2.8	46.95 ± 1.5	56.97 ± 1.1
Hemicellulose	17.12 ± 0.5	19.18 ± 0.7	36.96 ± 1.2	23.63 ± 0.9	25.03 ± 1.1	24.33 ± 0.8
Lignin	0.42 ± 0.02	0.05 ± 0.02	0.12 ± 0.04	17.05 ± 0.7	20.05 ± 0.9	20.11 ± 0.9
Ash	0.08 ± 0.004	0.21 ± 0.06	12.11 ± 0.6	19.91 ± 1.1	22.80 ± 1.3	16.54 ± 0.9
Extractives	0.54 ± 0.03	0.33 ± 0.02	0.33 ± 0.02	1.39 ± 0.05	1.69 ± 0.06	1.72 ± 0.07
Moisture	1.81 ± 0.09	1.74 ± 0.08	2.01 ± 0.18	1.61 ± 0.14	1.50 ± 0.09	1.99 ± 0.08

The lignin content is very low (< 0.5 percent) in WP samples (1-3) due to the bleaching process which is also related to the white color of the samples. In contrast, lignin is present in a relatively high

percentage in all of the RCF samples. The gray color of the RCFs corresponds to the remaining inks used in newspaper printing.

The highest ash content was determined in the RCF samples (4-6), ranging from 16 to 23 percent. The WP sample (3) also shows a higher ash proportion in comparison to the samples of the first set.

A decrease in lipophilic extractives quantity in all WP samples in comparison with the RCF samples was measured. By comparing the results of both sample sets, we clearly observed a better quality in WP samples 1 and 2.

Low moisture content values in the samples were found (approximately 1.5-2 wt.%).

3.2 Physical Properties

The results of the selected physical properties of the WP and RC fiber samples are given in Tab. 2.

3.2.1 Density and Bulk Density

The properties of the WP and RCF samples as bulk and porous substances are described by density and bulk density (Tab. 2). Density is an important material parameter since it affects other properties such as thermal conductivity and mechanical properties. The absolute density excludes all of the pores and therefore it is a measure of the solid matter of the fiber [30]. It is evident that density values are determined by the representation of the individual constituents in the cellulosic samples. The lowest density value was found in sample 1 (1508 kg/m^3), which had the highest content of cellulose (81.99 percent); this result was in accordance with the reported density value of pure cellulose (1592 kg/m^3). As shown in Fig. 2, the increasing trend in densities is caused by the content of non-cellulosic components, such as hemicelluloses, lignin and ash. The calculated value of the correlation coefficient (0.9854) shows a strong relationship between both of the mentioned variables. As is known, various physical properties are directly or indirectly influenced by the chemical composition of cellulosic fibers [31].

Table 2: Properties of Greencel cellulosic fibers (WP: 1-3; RCF: 4-6)

Characteristics of cellulosic fibers	Cellulosic fiber samples					
	1	2	3	4	5	6
Density (kg/m^3)	1508 ± 28	1524 ± 20	1831 ± 19	1843 ± 22	1966 ± 23	1943 ± 21
Bulk density (kg/m^3)	60 ± 2	40 ± 3	80 ± 4	75 ± 4	55 ± 3	40 ± 2
Max. fiber length (μm)	500 ± 25	1000 ± 40	500 ± 25	400 ± 15	600 ± 20	1200 ± 55
Dry matter (%)	93 ± 1	93 ± 1	90 ± 1	93 ± 1	93 ± 1	93 ± 1
pH	6 ± 1	6 ± 1	7 ± 1	7 ± 1	7 ± 1	7.5 ± 1
Average fiber width D (μm)	21.7 ± 2.2	21.3 ± 2.6	21.8 ± 2.3	29.5 ± 2.1	30.9 ± 1.5	29.0 ± 2.0
Average fiber length L (μm)	504 ± 24	514 ± 15	640 ± 31	556 ± 29	701 ± 31	796 ± 29
Aspect ratio L/D (-)	23.2	23.6	30	18.8	22.7	27.5
Thermal conductivity×10^{-4} (W/m.K)	674 ± 32	664 ± 38	656 ± 43	634 ± 22	599 ± 27	595 ± 30
Volume heat capacity×10^{-6} (J/m^3.K)	0.1454	0.1472	0.1818	0.2097	0.1785	0.1709
Thermal diffusivity×10^6 (m^2/s)	0.4639	0.4377	0.3827	0.3024	0.3354	0.3478

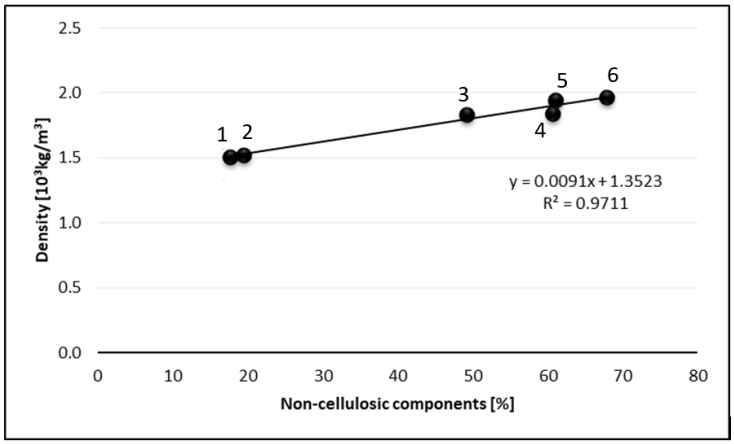

Figure 2: Density *vs.* total content of non-cellulosic components of the WP (1-3) and RCF (4-6) samples

The bulk density of WP and RCF samples reached their average values ranging from 40 to 80 kg/m^3. It is generally known that cellulosic fibers are low bulk density, closed-air polymeric materials in a porous structure. Therefore, the bulk density is always lower than the density. Fig. 3 shows that bulk density increases with decreasing average fiber length in the studied range of variables. The calculated value of the correlation coefficient (0.7663) confirms a moderate dependence between both of the mentioned variables.

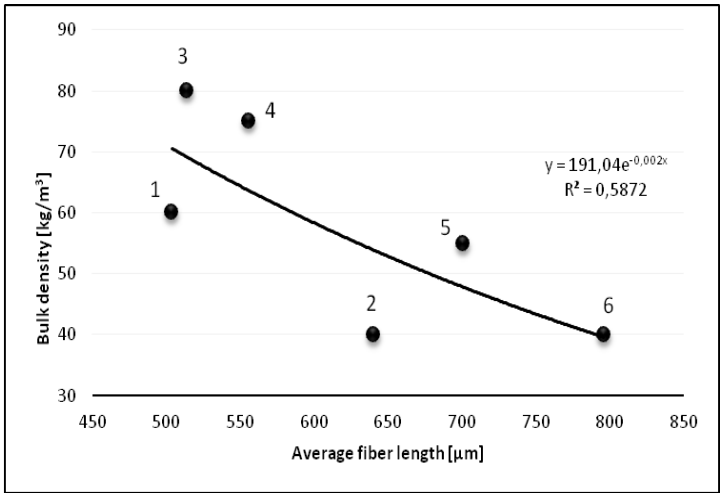

Figure 3: Bulk density *vs.* average fiber length of the WP (1-3) and RCF (4-6) samples

3.2.2 Dimensions and Morphology Study

Dimension data of cellulosic fibers in Tab. 2 show heterogeneity in the fiber sizes of the RCF samples in comparison to the WP samples. The histogram showing the frequency of fiber lengths distribution of WP and RCF samples is in Fig. 4. Two fractions have a majority representation (200-500 μm and 500-100 μm). The highest portion (54.7 and 52.8 percent) of the fraction with the smallest fiber length (200-500 μm) is recorded for the samples 1 and 2. RCF samples (4-6) and WP sample (3) have lower portion of this fraction (48.1 to 33.3 percent) in the order of samples (4 > 5 > 3 > 6). The portion of the second fraction (500-1000 μm) is very similar (42.4-44.8 percent) in five samples except for the sample 3. These differences in the fiber lengths distribution are reflected by the average fiber length (Tab. 2). The lowest average fiber lengths were measured for WP samples 1 and 2 (504 and 514 μm) and higher values (by 8-56%) were obtained for RCF samples (up to 796 μm) and sample 3 (640 μm).

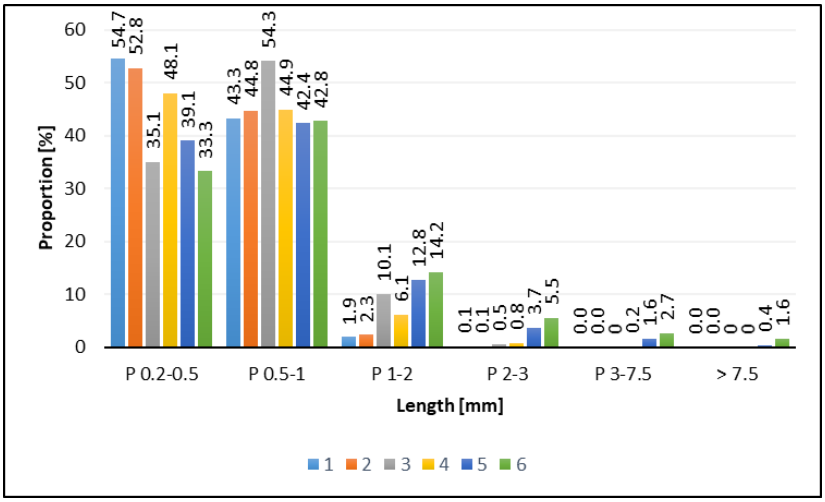

Figure 4: Histogram of fiber length fractions of WP (1-3) and RCF (4-6) samples

As shown in Tab. 2, the same values of the average width of the fibers in the samples (bleached wood pulp) were found (approximately 21-22 μm), but the RCF samples are thicker (approximately 29-31 μm). The cause of this phenomenon is probably related to inorganic impurities. The heterogeneity in the fiber sizes is also reflected by the aspect ratio of the studied fiber samples. L/D ratio is in the range of 18.8-30.

As can be seen from the SEM micrographs in Fig. 5, it was difficult with this method to determine the correct length of fibers in the samples, mainly in the RCFs because of their irregular shape, wide distribution of particle size, aggregation of fibers and presence of fiber fragments.

Significant changes on the fiber surfaces of the examined WP and RCF samples were observed. A comparison of the WP and RCF samples´ micrographs (Fig. 5) shows that bleaching treatment of fibers affects the quality of the fiber surfaces. More homogeneous and smooth fiber surfaces were observed in samples 1 and 2 than in sample 3. This finding relates to the high surface purity of the fibers corresponding to the cellulose content. The topography of the fiber surface of these samples does not show the presence of surface impurities compared to the native form of cellulose fibers. From the micrographs 4-6 in Fig. 5, a greater heterogeneity on fiber dimensions and the roughness of the fiber surface due to the presence of fiber fragments and impurities is clearly observed in the RCF samples (cellulose content approximately 47-57 percent). The fragments are formed by the mechanical damage to the fibers due to the recycling process of waste paper. The impurities in the RCF samples originate from paper-making processes by means of different additives, inks, and fillers.

The results of EDX elemental analysis of selected wood pulp and recycled fibers are shown in Fig. 6. The elemental analysis of the fiber samples with lower cellulose content (samples 3 and 4) revealed the presence of calcium (Fig. 6(b)), aluminium and silicon (Fig. 6(c)). The spectrum of WP sample 1 (Fig. 6(a)) was the same as the spectrum of sample 2 and contained only the peaks attributed to carbon and oxygen. The peaks observed at energy levels of 2.1 keV belong to the gold from the sample covering.

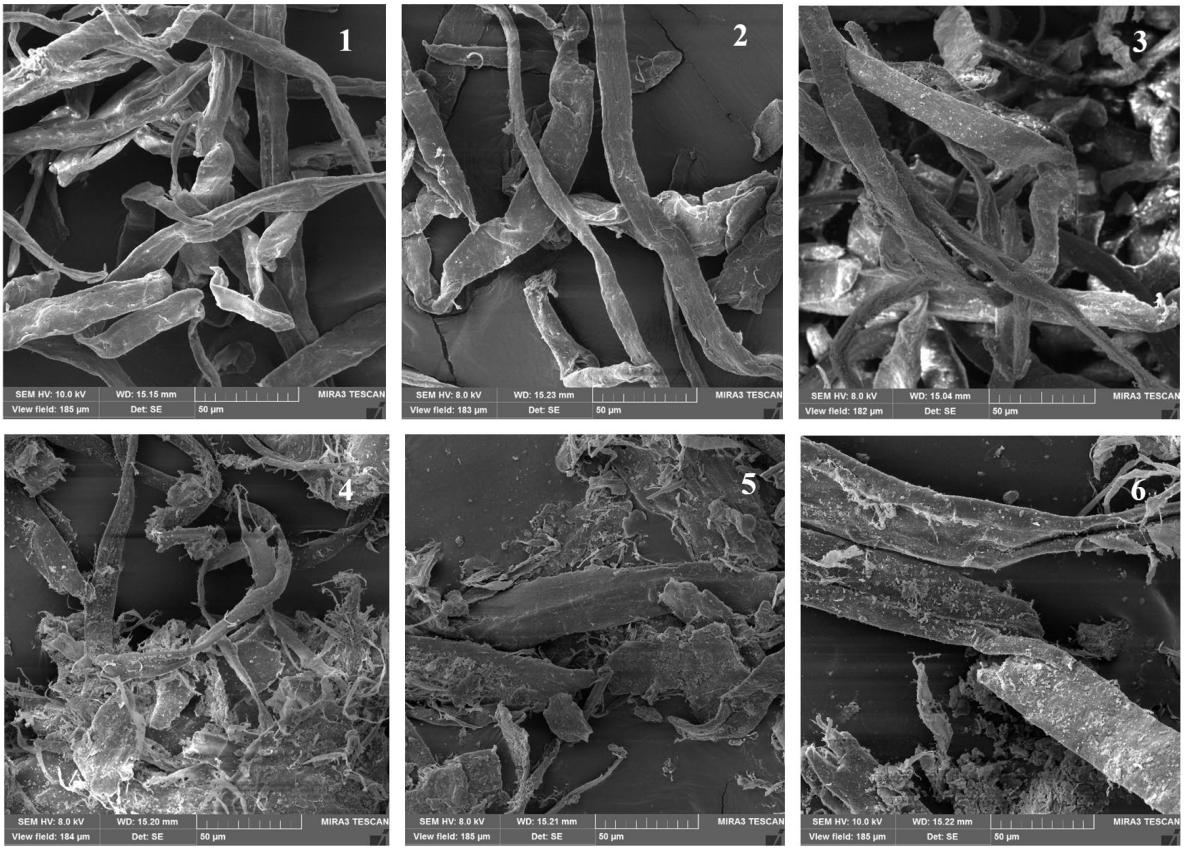

Figure 5: SEM micrographs of cellulosic fiber samples: WP (1-3) and RC (4-6); magnification = 1500x

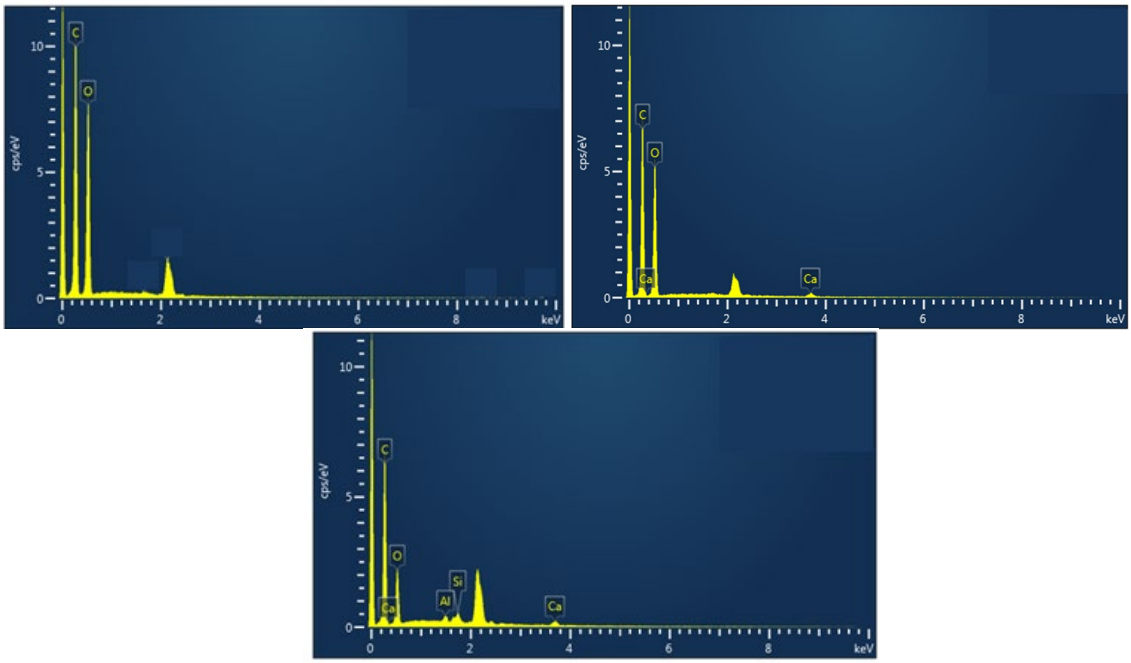

Figure 6: EDX analysis of WP sample 1 (a) and RCF samples 3 (b) and 4 (c)

3.2.3 Specific Surface Area and Pore Characteristics

The specific surface area and micro pore volume radius are parameters used for characterization of porous materials. In this work, various empirical models were applied to analyze the surface and pore characteristics calculated using the BET equation for WP and RCF samples. As seen in Tab. 3, the values of the specific surface area of fibers measured by monolayer and multilayer adsorption are different.

Table 3: Specific surface area and pores characteristics of Greencel cellulosic fibers (WP: 1-3; RCF: 4-6)

Parameter	Cellulosic fiber samples					
	1	2	3	4	5	6
Langmuir specific surface area (m^2/g)	18.4	19.4	19.2	21.5	17.2	14.0
BET specific surface area (m^2/g)	8.26	9.41	7.42	9.48	8.63	7.60
HK total micro pore volume ($10^3\ cm^3/g$)	2.16	2.17	1.71	2.44	2.70	2.62
HK pore radius (nm)	7.14	1.84	7.01	6.99	7.01	1.84
DR micro pore volume ($10^3\ cm^3/g$)	1.01	11.62	7.32	9.58	5.69	8.13
DR micro pore radius (nm)	8.89	8.65	8.28	5.03	4.06	4.12
NLDFT cumulative pore volume ($10^3\ cm^3/g$)	4.00	12.65	11.37	20.64	12.98	22.06
NLDFT pore radius (nm)	1.06	1.66	3.11	2.71	1.66	2.08
SF cumulative pore volume ($10^3\ cm^3/g$)	2.32	2.80	1.82	2.59	2.83	2.72
SF pore radius (nm)	1.75	1.75	1.75	1.75	1.75	1.75

Langmuir specific surface area values are higher than BET values due the fact that BET theory ignores non-homogeneity of the surface and the measured surface area does not completely reflect a real internal surface [32]. On the other hand, BET surface area presents the external surface area in the range from 7.42 to 9.48 m^2/g. The surface area also depends on the number active sites on the fiber surface. It is evident that changes in the chemical composition on the fiber surface affect the specific surface area value but also the pore structure. The lowest value of the specific surface area was measured for sample 3, which corresponds to the highest hemicellulose content (Tab. 2). This finding is supported by the results found in a previous publication [33], where the changes in pore structure and in pulp swelling behavior after recycling were explained by the presence of a significant variety of hemicellulose content in the pulp samples. The porous structure of native cellulosic fibers is one of the important factors influencing their properties such as their accessibility during chemical reactions, swelling and mechanical properties [33]. The cumulative pore volume and average pore size values are determined by the measuring and calculating methods used. The reported values of these pore characteristics are different due to fundamental differences in measuring techniques and sample materials. As is known, pores creation also takes place during the pulping and bleaching processes, when lignin and hemicelluloses are removed from the cellulose fiber wall structure [34]. Many disordered and connected pores can be formed in meso-porous materials. Therefore, some models overestimate or underestimate their value and are not reliable. The NLDFT model can provide realistic pore volume estimation and seems to be suitable for meso- and micro-porous materials [32]. The cumulative pore volumes determined by this method range between 4×10^{-3} and $22 \times 10^{-3}\ cm^3/g$ with the lowest value coming for sample 1 and the highest value belonging to sample 6. The average pore radius is estimated from the pore volume assuming cylindrical pore geometry. The average values of the NLDFT pore radius were found in the range of 1.06 to 3.11 nm. While samples 1, 2 and 5 have an average pore radius belonging to micro-porous material, this parameter for samples 3, 4 and 6 is higher than 2 nm and characterizes a meso-pore radius. Sample 3 with the highest value of average pore radius (3.11 nm) shows the lowest values of HK total micro pore volume ($1.71 \times 10^{-3}\ cm^3/g$) and specific surface area ($7.42\ m^2/g^{-1}$).

3.2.4 Crystalinity and Crystallite Size

The XRD patterns of the cellulosic samples (Figs. 7 and 8) show the peaks attributed to cellulose I [35]. As is known, the crystalline structure of cellulose I is a mixture of two distinct crystalline forms: celluloses I_α (triclinic) and I_β (monoclinic), which are in their ordered and amorphous phases. The relative amounts of celluloses I_α and I_β vary with the source of the cellulose.

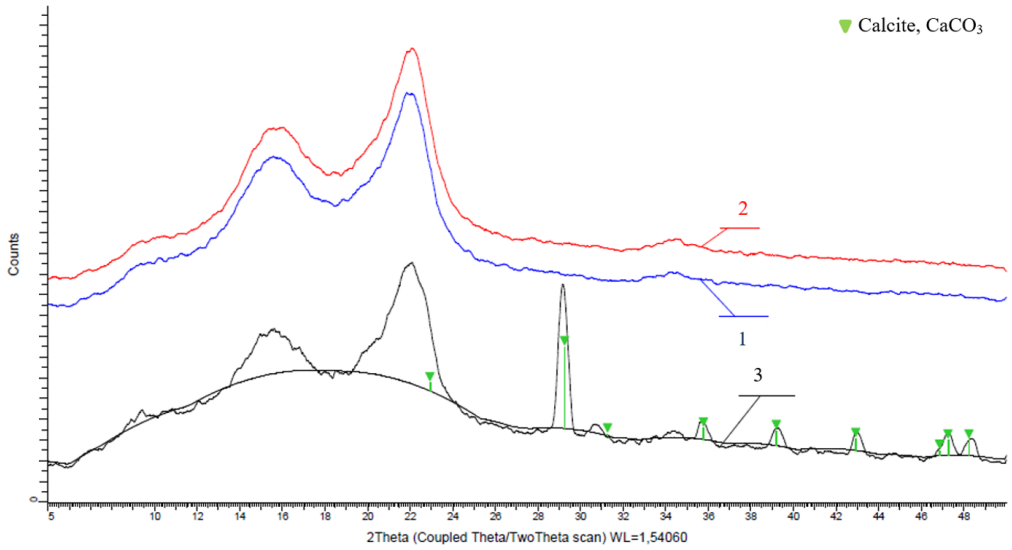

Figure 7: XRD diffractograms of WP fiber samples (1-3)

The XRD patterns of the WP and RCF cellulosic samples present three characteristic peaks of cellulose. The intensity of the main (002) peak between 20° and 24°, with a maximum at 2θ = 22.6°-22.8° represents both crystalline and amorphous cellulose; the minimum height at 2θ = 18.5° ($I_{110} = I_{AM}$) corresponds to the amorphous phase [33]. Another peak of lower intensity is located between 14° and 18°, with a maximum at 16.4°-16.6°. A further peak of weak intensity is seen at approximately 2θ = 34°. In previous papers [36], similar results have been reported. The XRD patterns shows that the ordered structure of the crystalline region in the cellulosic samples (1 and 2) does not seem to be disrupted by the bleaching process in comparison to other samples. As seen in Figs. 7 and 8, the lower intensities of the three peaks attributed to cellulose were found for the RCF samples with lower cellulose content (3-6) in comparison to high-purity WP samples (1 and 2). Except for the characteristic diffraction lines of cellulose in Figs. 7 and 8, the presence of other peaks was identified. The peaks observed on the XRD pattern of samples 3 and 5 at 2θ = 29.2°, 2θ = 35.7°, and higher 2θ angles (Figs. 7 and 8) belong to calcium carbonate (calcite) [37]. In Fig. 8, the peaks observed at 2θ = 12.19° and 24.62° in the diffraction patterns of RCF samples (4-6) are attributed to aluminium silicate hydroxide (kaolinite; $Al_2Si_2O_5(OH)_4$) [38]. Calcite and kaolinite belong to the most used mineral fillers in the paper-making process. These results are in a good agreement with the results of the elemental analysis presented in Section 3.2.3.

The calculated values of CrI, as one of the most significant crystalline structure parameters of studied cellulosic fiber samples, are presented in Tab. 4. The CrI values for WP samples (1 and 2) are approximately 51-52 percent, while for RCFs and WP sample (3), the results are decreased to 44 percent. The results listed in Tab. 4 indicate that the crystallite size increases with the increasing crystallinity index of bleached fibers (WP samples) and their purity [39]. On the other hand, the CrI index of the RCF samples has the opposite character in comparison with the CrI of WP samples. Based on these facts and the data in the literature [40], the crystalline structure of cellulose depends on its history as well as the source and the processing of fibers. As stated in the paper [40], the chemical treatment of natural fibers can influence the crystallinity of cellulose.

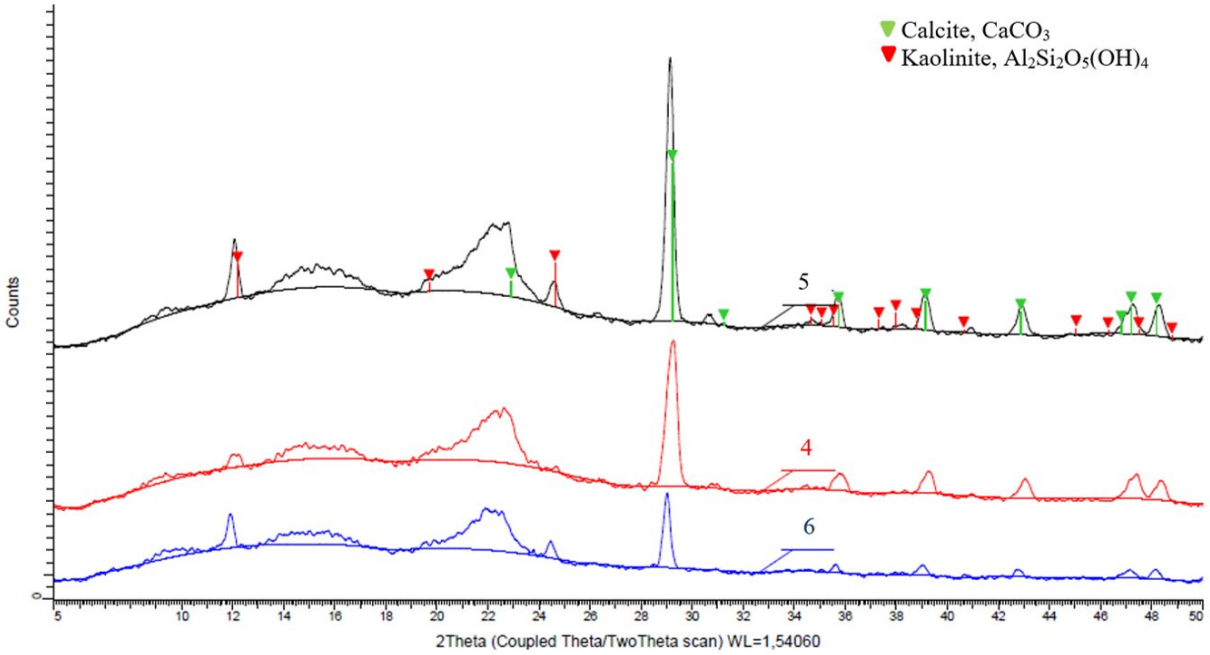

Figure 8: XRD diffractograms of RCF samples (4-6)

Table 4: Crystallinity index and crystallite size of Greencel cellulosic fibers (WP: 1-3; RCF: 4-6)

Sample	Crystallinity index CrI (%)	Crystallite size L (nm)
1	51.07	4.49
2	52.60	4.56
3	49.06	4.29
4	48.89	4.94
5	50.86	4.90
6	44.11	5.21

3.2.5 Degree of Cellulose Polymerization and Polydispersity Index

Size exclusion chromatography (SEC) is an extremely useful type of analysis to characterize the polymer structure of cellulose. This method allows determine an important structural parameter, degree of polymerization (DP) that significantly influences the mechanical properties of cellulose [41]. According to paper [42], an increase in the DP of cellulose leads to an improvement in the strength properties of the fibers. The DP actually represents the average cellulose chain length that is often expressed in terms of the molecular mass of the polymer chain, and it is related to the relative molecular mass of the monomers and the number of monomers connected in the chain. The polymer chains, however, have unequal length, so the polymer exists as a distribution of chain lengths and molecular masses. The results of the number- and weight-average molecular mass (Mn and Mw), polydispersity index (PDI) and degree of polymerization (DP) are displayed in Tab. 5. The results show certain differences in the molecular mass depending on the various origins of the tested cellulosic fibers in accordance with [43]. The WP samples have lower Mn and Mw values in comparison to the RCFs; this is probably related to the impurities. According to previous work [44], the Mw values in wood pulp approximately reached 100,000 g/mol. The Mw values of the investigated WP and RCF samples are higher than those previously published.

Table 5: Comparison of the values of the weight-average molecular weight (Mw), number-average molecular weight (Mn), polydispersity index (PDI) and degree of cellulose polymerization (DP) of WP and RCF samples

Cellulosic sample		Mw (g/mol)	Mn (g/mol)	PDI	DP
WP	1	175,642	26,233	6.70	1,084
	2	181,164	26,731	6.78	1,118
	3	184,006	27,840	6.61	1,136
RCF	4	190,475	27,637	6.92	1,176
	5	192,747	31,276	6.16	1,190
	6	208,100	33,045	6.30	1,285

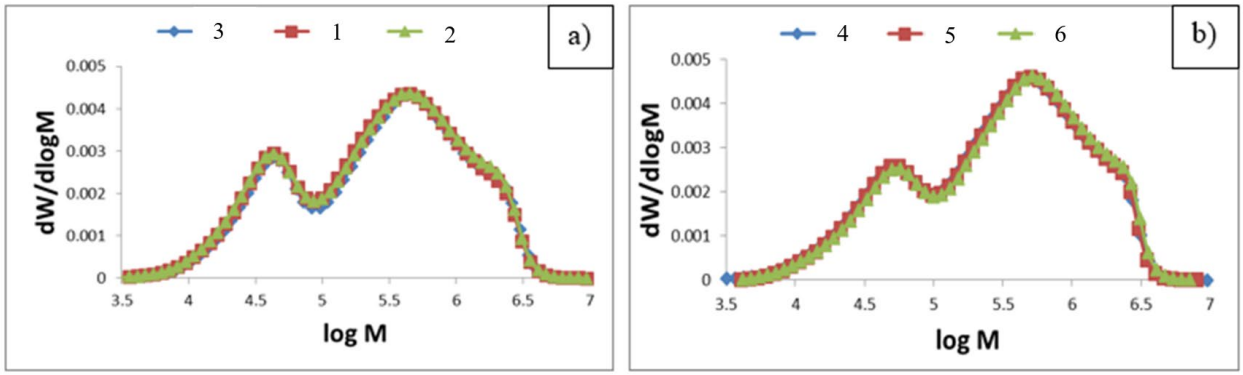

Figure 9: Cellulose weight-molecular mass distribution of WP (a) and RCF (b) samples

As is shown in Tab. 5, the DP values are in the range of 1,084 to 1,285. Higher DP values were found for RCFs in comparison to the DP of cellulosic fibers from WP. Figs. 9(a) and 9(b) show the weight-molecular mass distribution curves of samples representing two sets of cellulosic fibers. As was observed from the bimodal distribution of the molecular masses, a large portion represents high molecular mass fractions and a smaller portion belongs to low molecular mass fractions. No significant differences were observed between the PDI values of WP (6.61-6.78) and RCF samples (6.16-6.92).

3.2.6 Chemical Functional Groups

In addition to compositional determination, FTIR has been used to study the structure of cellulosic fiber samples. The FTIR spectra of WP and RCF samples, in comparison to reference sample in Figs. 10 and 11, revealed bands in two wave number regions that are characteristic of the presence of cellulose (3660-2800 cm^{-1} and 1650-400 cm^{-1}) [45]. The observed differences in spectra allow for identifying the structural changes. The spectra of the WP samples are comparable to a reference sample (Fig. 10), while differences in absorption band intensities and the presence of new peaks in the spectra of RCF samples are observed (Fig. 11).

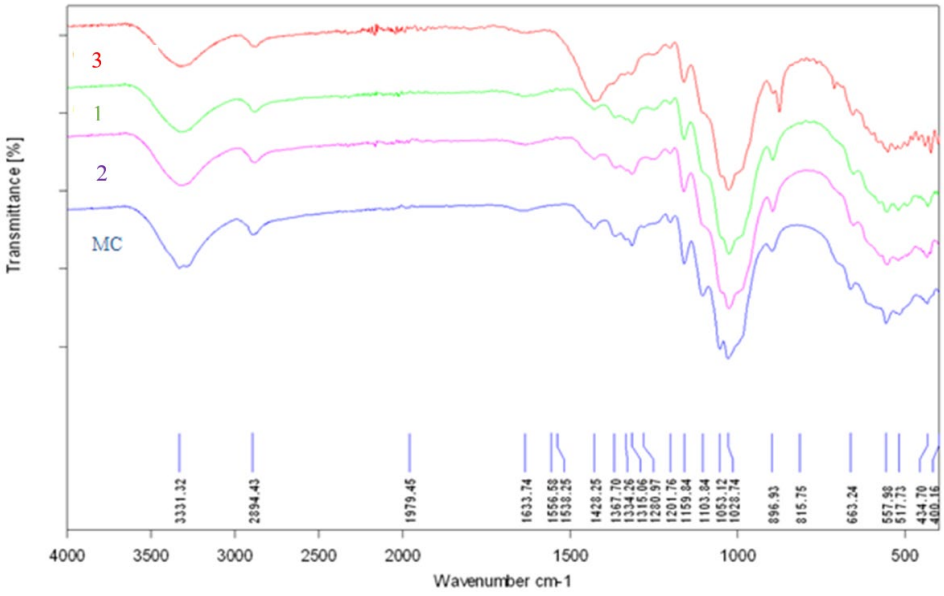

Figure 10: FTIR spectra of WP samples (1-3) in comparison to microcrystalline cellulose (MC)

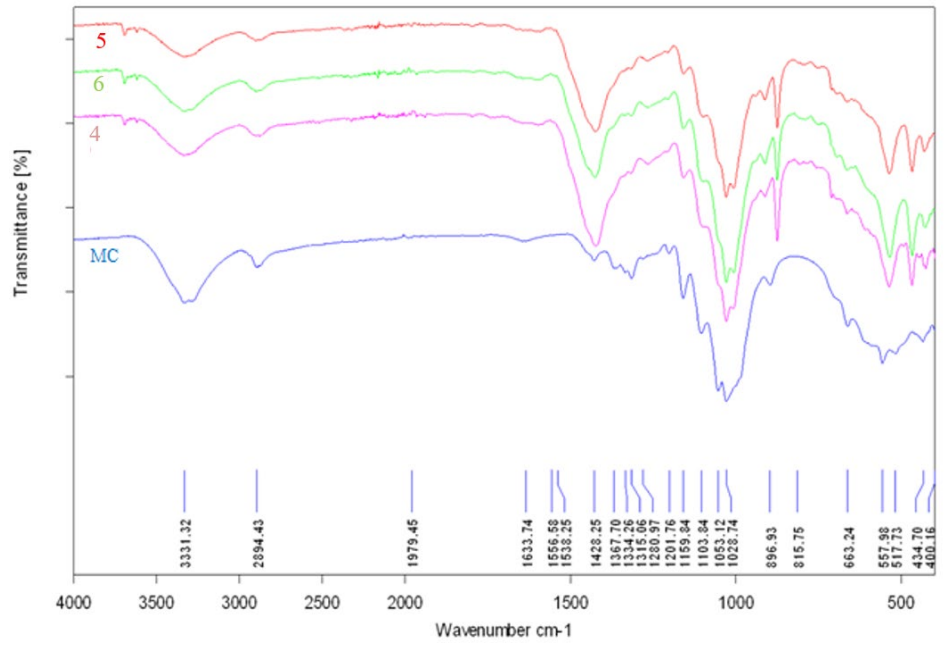

Figure 11: FTIR spectra of RCF samples (4-6) in comparison to microcrystalline cellulose (MC)

The identification of the absorption bands observed in the spectra of the investigated cellulosic fibers is very similar to that presented for hemp hurds in our previous work [21].

The absorption peaks in the wavelength range 3660-2900 cm^{-1} are characteristic for the stretching vibration of O-H and C-H bonds in polysaccharides. The absorption peak at 3331 cm^{-1} corresponds to the vibration of the O-H bond, and this broad peak includes inter- and intramolecular hydrogen bond vibrations in cellulose [46]. The band at 2894 cm^{-1} is attributed to the C-H bond vibrations of all hydrocarbon constituents in polysaccharides [47].

In the region of 1630-900 cm^{-1}, many absorption bands corresponding to the vibration of functional groups that present cellulose are observed. The peaks located at 1633 cm^{-1} belong to the vibration of water molecules absorbed in cellulose [47]. The absorption bands at 1428, 1367, 1334, 1027, and 896 cm^{-1} are attributed to the stretching and bending vibrations of the $-CH_2$ and -CH, -OH, and C-O bonds vibrations in cellulose [48]. The peak intensity present approximately 1420-1430 cm^{-1} is associated with the amount of the crystalline cellulose, while the peak at 896 cm^{-1} is assigned to the amorphous regions in cellulose [25]. For the spectrum of sample 3 (Fig. 10), visible differences appeared. There can be observed some modifications of the signals at 1428 cm^{-1}, 896, 875, and 712 cm^{-1}. A broad peak at 1428 cm^{-1} includes not only the vibrations of the $-CH_2$ and CH bonds from cellulose but also the vibration of C=O bonds in the carbonate ion (CO_3^{2-}). The band typical for CO vibration in pure $CaCO_3$ is visible at 1475 cm^{-1}. Furthermore, two peaks of weak intensity at 875 and 712 cm^{-1} also belong to the C=O bond vibrations in carbonate anions. The FTIR spectra of the RCF samples in Fig. 11 are very similar to the spectrum of WP sample 3 (Fig. 10). However, the peaks attributed to the bonds present in the kaolinite structure were additionally observed. Kaolinite, as a clay layered aluminosilicate mineral, consists of tetrahedral (Si^{4+}, Al^{3+}) and octahedral (Al^{3+}, Fe^{3+}) layers. The absorptions at 3697, 3669, 3645, and 3620 cm^{-1} are typical for the Al ...O-H stretching vibration of Al in octahedral as well as O-H stretching [49]. The band at approximately 1100-1010 cm^{-1} is assigned to Si-O stretching vibrations. The peaks at 936-914 cm^{-1} correspond to the Al-OH bending vibration of kaolinite [50]. The bands at 914 cm^{-1} and peaks in the range of 800-784 cm^{-1} are attributed to the deformation bands of the OH bonds linked to Al^{3+}, and Al^{3+} and Mg^{2+} ions, respectively. The peaks at 540 and 470 cm^{-1} are attributed to Si-O-Al stretching and Si-O-Si bending vibration (inter tetrahedral bridging bonds in SiO_2). These results imply the presence of calcium carbonate [51] and kaolinite in cellulosic fiber samples as impurities derived from the used filler in paper-making, which corresponds to cellulose purity (Tab. 1).

3.2.7 Thermal Degradation Characteristics

Thermal analysis provides information on the thermal stability of a material as well as heat release during simultaneous heating. The mass loss curves (TG), DTG and DSC curves of the six tested cellulosic fiber samples in an inert atmosphere of nitrogen are shown in Figs. 12-14. Tab. 5 summarizes the parameter values obtained from DSC analysis.

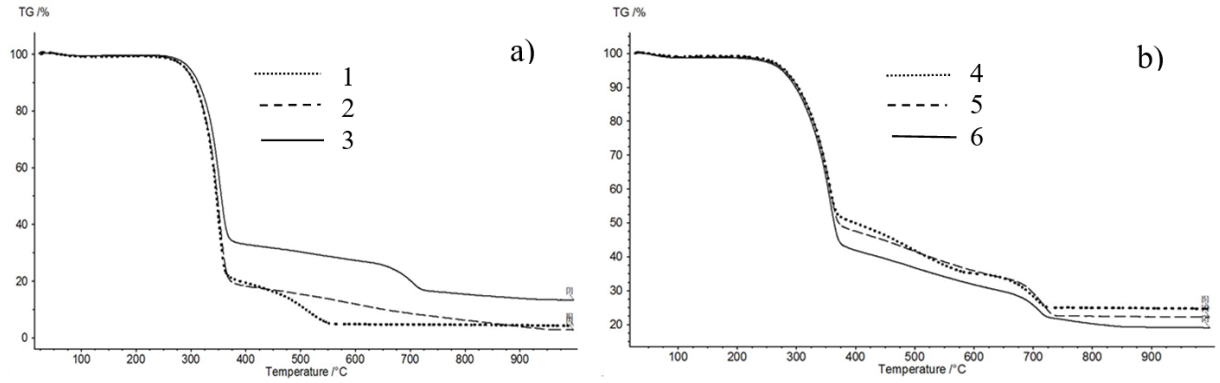

Figure 12: TG curves of WP (a) samples (1-3) and RCF (b) samples (4-6)

As seen in Figs. 12-14, the thermal decomposition process of cellulosic fiber samples can be divided into three stages. As is known, the decomposition of cellulosic samples is a complex process involving a series of consecutive reactions. There were some difficulties in characterizing the decomposition behavior of substances forming cellulosic fiber samples and recognizing the progress of individual degradation actions occurring during their heating as a result of the complexity of its microstructure [25]. We have encountered a similar problem in the thermal degradation studying of organic compounds present in hemp hurds samples [52]. While only slight differences were observed between the samples in DTG curves during the course of the degradation (Figs. 13(a) and 13(b)), significant differences were found in the

DSC curves (Figs. 14(a) and 14(b)). The TG, DSC, and DTG curves of the RC and WP fiber samples, obtained by analysis in a nitrogen atmosphere, show a very weak initial endothermic peak between 25 and 127ºC, where a small weight loss (0.55-1.22 wt.%) was recorded. In this temperature range, the evaporation of physically adsorbed water (moisture) from the fiber structure occurs. The moisture content in the samples determined gravimetrically ranged from 1.5 to 2 percent (Tab. 2). Owing to the hygroscopic nature of the fibers, the amount of moisture is highly dependent on the ambient humidity and the manner in which the fibers are handled [53]. Hemicelluloses and lignin constituting the major part of the amorphous phase play an important role in the storage of moisture in fibers. As shown in [54], a portion of the bound water in the fibers depends significantly on the crystallinity degree of the cellulose.

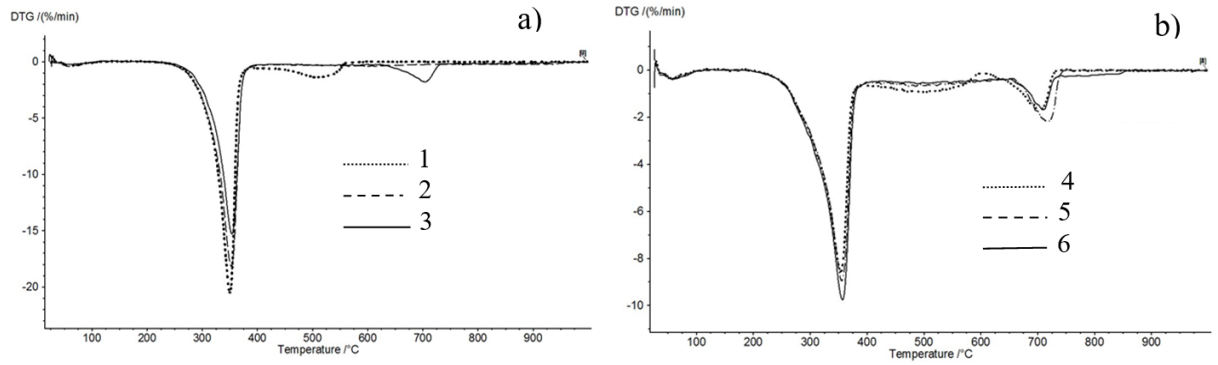

Figure 13: DTG curves of WP (a) samples (1-3) and RCF (b) samples (4-6)

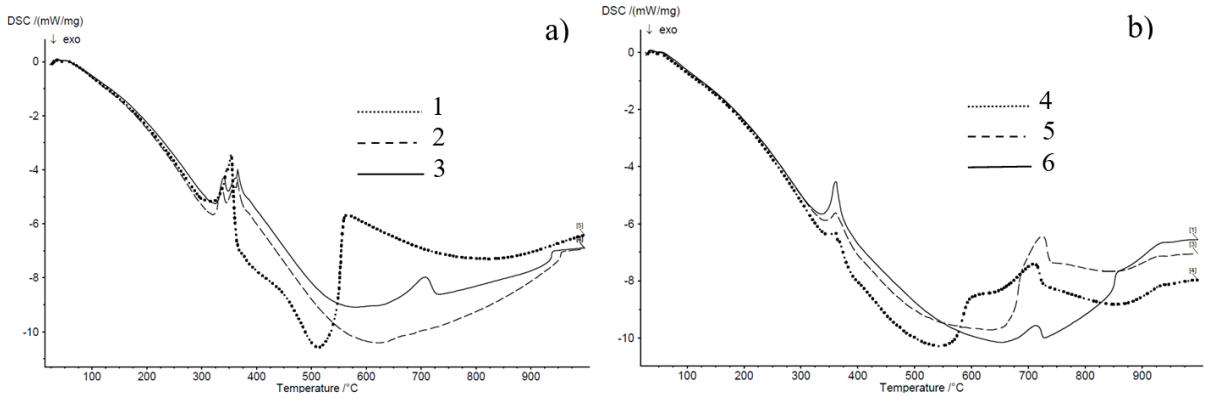

Figure 14: DSC curves of WP (a) samples (1-3) and RCF (b) samples (4-6)

In the second stage, the greatest mass loss between 206°C and 400°C was recorded due to the devolatilization process being the main decomposition process of cellulosic fiber samples. It has been widely accepted that the primary thermal decomposition of cellulosic materials occurs between 200°C and 400°C [55]. In this temperature range, the organic components are gradually released. Cellulose decomposition as an endothermic process in an inert atmosphere mostly starts in the amorphous regions [56]. The endothermic peak on the DSC curves (Figs. 14(a) and 14(b)) and one significant peak on the DTG curves (Figs. 13(a) and 13(b)) at a temperature of approximately 350°C is accompanied by a mass loss of 66.71, 78.62, 80.94 wt.% for WP (samples 1-3) and 48.45, 50.85, 56.13 wt.% for RCF (samples 4-6). This mass loss is a result of the decomposition of the major components of the fibers. As demonstrated in [57], the temperature of the hemicellulose depolymerization ranged between 180°C and 350°C, but the decomposition of the largest portion of hemicelluloses occurred in the narrow temperature range of 180-200ºC. Cleavage of the glycosidic linkage of the cellulose units was observed between 275°C and 350°C [58]. The higher onset temperatures of cellulose decomposition (Tab. 5) indicate its higher thermal

stability in comparison to hemicelluloses in accordance with a previous paper [59]. According to work [60], higher cellulose resistance to a thermal treatment is probably due to the presence of a much higher amount of intra- and intermolecular hydrogen bonds between the cellulose chains, which can lead to more ordered and packed regions in the cellulose structure.

Table 5: Thermal parameters of cellulosic fiber samples (WP: 1-3; RCF: 4-6) obtained from DSC analysis

Sample	Onset temperature (°C)	Peak temperature (°C)
1	339.3	339.9
	345.5	346.1
	-	355.0
	550.0	557.4
2	328.5	328.3
	-	338.0
	363.2	365.0
	-	625.0
3	332.1	332.0
	-	340.8
	363.8	365.8
	-	590.1
	695.1	710.5
4	350.7	361.9
	720.7	729.2
5	351.7	360.9
	368.1	368.8
	575.3	593.5
	-	714.7
6	350.3	362.0
	693.4	713.6
	850.5	854.3

Lignin degradation simultaneously proceeds with the decomposition of cellulose and hemicelluloses in the first and second temperature range, but its temperature range is broader than for the hollocellulose components. The decomposition of residual lignin starts at 160°C and slowly continues until its completed decomposition at 900°C [59].

One broad exothermic peak on the DSC curves (Fig. 14) represents the third decomposition stage between 375 and 600°C. In the case of sample 1 (Fig. 13(a)) and sample 5 (Fig. 14(b)), there are peaks in the temperature ranges of 431°C-568°C and 388°C-604°C, leading to further mass loss of 12.71 wt.% and 15.66 wt.%, respectively. These exothermic peaks correspond to the residual lignin decomposition and kaolinite dehydroxylation that occurs between the temperature 450°C and 650-700°C [61]. Kaolinite decomposition occurs in the temperature range of 457-711°C with maximum heat release at 519°C [62].

The maximum peak of the release of hydroxyl groups at approximately 515-540°C was recorded for samples 1 and 5, which is in a good accordance with the findings of paper [62]. The thermal behavior of kaolinite at a higher temperature is described via a sequence of reactions of the transformation of the crystalline aluminosilicate phase ($Al_2O_3.2SiO_2$) into $2Al_2O_3.3SiO_2$ and amorphous SiO_2 (925-1050°C).

In the temperature range of 604°C-747°C, the decomposition of residual kaolinite alongside calcite proceeds in accordance with the papers [62]. For WP sample (3) and all of the RCF samples (4-6), a small endothermic peak with maximum at 710, 729, 715, and 714°C, respectively, was found. This could be related to calcite decomposition. In this temperature range, the mass loss of sample 3 was 10.19 wt.%, and 8.3, 9.96 and 10.04 wt.% for the RCF, respectively. The residues remaining after the thermal degradation of WP samples (1-3) were approximately 2.77, 4.22, and 13.35wt.%, respectively. For the

RCF samples (4-6), the residues were higher (22.10, 24.65, and 19.02 wt.%) in comparison to the WP residues. These residues correspond to inorganic components in the cellulosic fiber samples and their values are well correlated with the determined ash content by chemical analysis (Tab. 1).

3.2.8 Heat Transfer Characteristics

The values of the thermal conductivity, volume heat capacity and thermal diffusivity of the WP and RCF samples are introduced in Tab. 2. From a comparison of the thermal conductivities, it follows that more favorable values have been achieved for the RCF samples (0.0595-0.0634 W/m.K) than for the WP samples (0.0644-0.0674 W/m.K). As is generally known, polymers consisting of monomers of organic compounds have low values of this parameter; the value of 0.062 W/m.K was obtained for the regenerated cellulose fibers (viscose kind) [63]. There are also visible the differences between the volume heat capacity and the thermal diffusivity of the studied samples (Tab. 2). As is known, thermal properties of cellulosic fibers are influenced by many factors. Variables influencing their thermal conductivity are the morphology, molecular structure, porosity, density, crystallinity degree, crystal orientation angle and mobility of molecular chains in amorphous regions [64]. The differences in the source quality of waste paper affect the thermal conductivity of cellulose fibers. Obviously, the effect of the cellulose content, crystallinity and degree of polymerization as well as the porous fiber structure is reflected in thermo physical characteristics of the cellulosic fibers, as shown in Figs. 15 and 16.

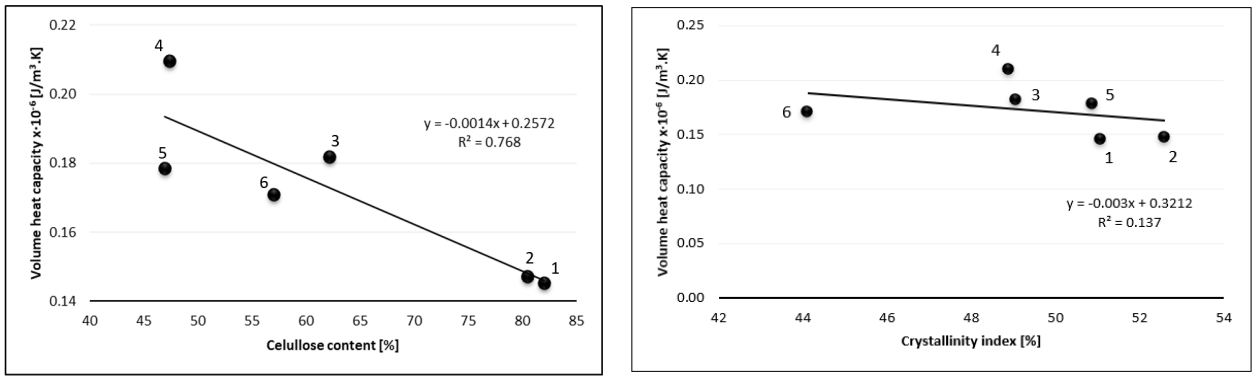

a **b**

Figure 15: Dependence of volume heat capacity on cellulose content (a) and crystallinity index (b) in Greencel fibers (WP: 1-3; RCF: 4-6)

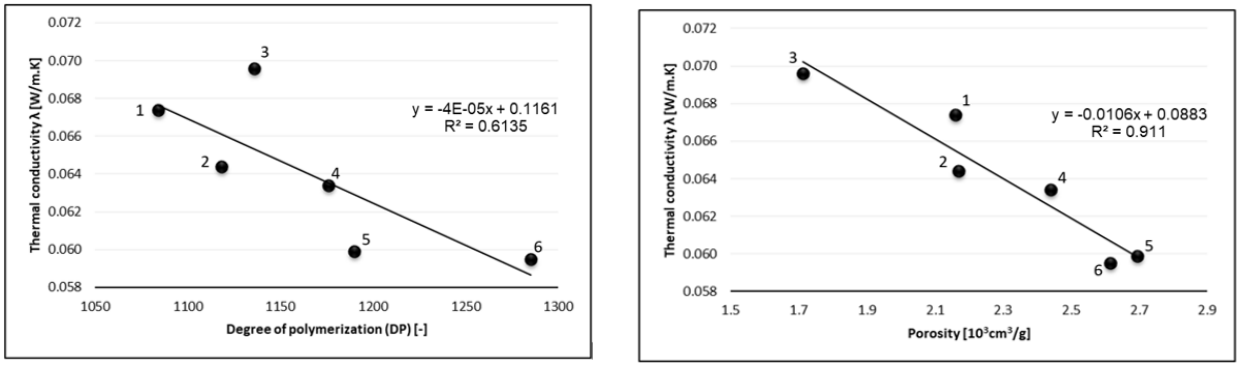

a **b**

Figure 16: Dependence of thermal conductivity on degree of cellulose polymerization and HK total micro pore volume of Greencel fibers (WP: 1-3; RCF: 4-6)

Testing the significance of a correlation coefficient based on comparing the calculated absolute and critical value for the linear dependences as shown in Figs. 15(a) and 16(b) showed that the calculated correlation coefficients (0.8764 and 0.9546, respectively) are approximately higher than the critical value of the correlation coefficient (0.8114) for a set of measured values at the selected significance level p = 0.05. There is a very strong dependence among the variables. The value of the correlation coefficient for the dependence of thermal conductivity on the degree of cellulose polymerization as shown in Fig. 16(a) was found to be lower (0.7833) than the critical value of the correlation coefficient but very close to this value. This result is related to a moderate dependence between both variables. The smallest force of statistical dependence expressed by the correlation coefficient (0.3700) was recorded between volume heat capacity and crystallinity index (Fig. 15(a)). Fig. 17 shows a very strong dependence (0.8828) between both variables. The waste paper cellulose fibers of lower quality contribute to a reduction in thermal conductivity values that can positively affect this parameter of fiber composite.

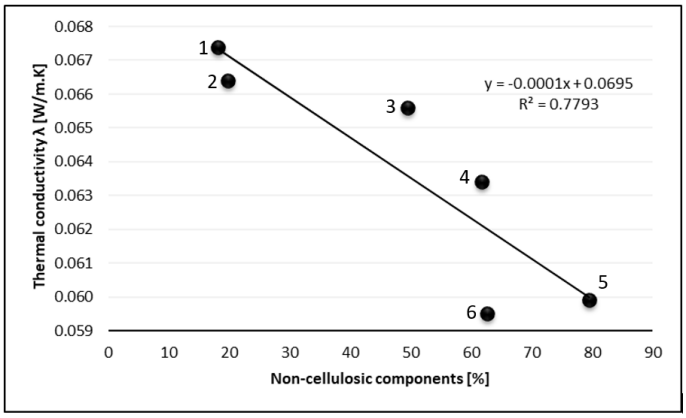

Figure 17: Thermal conductivity *vs.* content of non-cellulosic components in Greencel fibers (WP: 1-3; RCF: 4-6)

3.3 Mechanical Properties and Capillary Water Absorption of Fiber-Cement Mortars

To gain a complete picture of the response of fibers behavior in cement matrix, an investigation of compressive and flexural strength of fiber-cement mortars was carried out. The values of flexural and compressive strength of 28-day-cured fiber-cement mortars compared to the reference sample (without fibers) are in Tab. 6. As seen, the flexural strengths (5.1-5.3 MPa) of the cured mortars with cellulosic fibers are definitely lower than the values of compressive strength (28 MPa-34.2 MPa). No significant differences in flexural and compressive strengths between the mortar groups were recorded. A 17-32 percent decrease in the compressive strength values of all mortar samples compared to the reference mortar (RM) was observed. According to the standard requirement for interior plasters [27], the obtained values of compressive strength of 28-day-cured fiber-cement mortars are within the accepted range and can be assigned based on this strength parameter to class CS IV (≥ 6 MPa).

Table 6: Flexural and compressive strength of 28-day-cured WP and RC fiber-cement mortars

Strength parameter (MPa)	Fiber-cement mortar specimens						
	RM	1	2	3	4	5	6
Flexural strength	7 ± 0.4	5.3 ± 0.4	5.1 ± 0.3	5.1 ± 0.5	5.5 ± 0.2	4.9 ± 0.3	5.3 ± 0.3
Compressive strength	41.2 ± 3.7	34.2 ± 2.8	28.0 ± 2.0	30.8 ± 3.1	31.2 ± 1.9	28.8 ± 2.4	30.1 ± 2.7

Based on the measured values of the of capillary water absorption coefficient of 28-day-cured fiber-cement mortars, mortar sample with RCF (sample 2) reached a lower value of this parameter (0.23 $kg/m^2min^{0.5}$) compared to mortar with WP fiber sample 5 (0.26 $kg/m^2min^{0.5}$). This result also confirms the

suitability of recycled fibers for use in cement mortars. The recycled cellulosic fibers are characterized by a high content of inorganic substances having a natural adhesion to the cement particles.

Our next aim is to design recipe for plastering mortars based on cellulosic fibers, to optimize the mixture composition and to evaluate the final effect of a partial replacement of filler in the cement matrix by using different amounts of both kinds of cellulosic fibers on the mechanical, thermal and sorption properties of mortars in order to develop environmentally friendly plaster mixtures with good thermal insulation properties. To predict the fiber-cement material's stiffness, a deeper analysis of interfacial adhesion between fiber and matrix will also take place.

4 Conclusion

In this study, cellulosic fibers originating from bleached wood pulps and recycled waste paper were characterized according to their chemical and physical properties to determine their potential use as fillers in building composite materials. A morphological study revealed the differences in the quality of the surface of cellulosic fibers and in their fiber dimensions. The surfaces of the WP fibers were more homogeneous and smoother than the heterogeneous surfaces of the RC fibers, which were characterized by the roughness and the presence of impurities and fiber fragments. RCFs had a larger width, approximately 10 μm, in comparison to samples of bleached WP. Moderate exponential inverse dependence between bulk density of the samples and average fiber length was observed. Chemical analysis confirmed the higher portion of inorganic substances as well as the lowest cellulose amount, and the higher content of hemicellulose and lignin in the RCF samples in comparison to the WP samples with high holocellulose content (> 99 percent). The linear dependence between the density and content of non-cellulosic components was found. Lower crystalline cellulose contents and higher values of its degree of polymerization were found for RCFs in comparison to the cellulosic fibers from wood pulp.

Changes in the chemical composition, cellulose crystalinity and degree of polymerization of the investigated cellulosic fibers affected the physical properties of the fibers. The results of thermo physical properties showed that the heat transfer characteristics (thermal conductivity, volume heat capacity and thermal diffusivity) of the cellulosic fibers depended on their quality as expressed by their cellulose content, crystallinity and degree of polymerization as well as their porosity. In comparison, more favorable values of thermal conductivity were achieved with the RCFs (0.0595-0.0634 W/m.K) than for the WP samples (0.0644-0.0674 W/m.K).

The suitability of recycled cellulosic fibers for their use as fillers in plastering mortars (0.5 wt.% fiber content of the total weight of the filler and binder) has been confirmed by achieving the required compressive strength value (approximately 30 MPa). The recycled cellulosic fibers have been identified more suitable for the application in building materials than bleached wood pulps. These cellulosic fibers were characterized by a lower value of capillary water absorption and high content of inorganic substances having a natural adhesion to the cement particles.

Acknowledgement: This work was supported by the Slovak Scientific Grant Agency VEGA [Grant Nos. 1/0277/15 and 1/0222/19] and the Project Institute of Clean Technologies for Mining and Utilization of Raw Materials for Energy Use [Grant No. LO1406].

References

1. Mohanty, A. K., Misra, M., Drzal, L. T. (2002). Sustainable bio-composites from renewable resources: opportunities and challenges in the green materials world. *Journal of Polymers and the Environment, 10,* 19-26.
2. Thabang, H. M., Maya, J. J. (2017). Bio-based fillers for environmentally friendly composites. In: Thakur, V. K., Thakur, M. K., Kessler, M. R. (eds.), *Handbook of composites from renewable materials*, vol. 1, pp. 243-270. Beverly: Scrivener Publishing LLC.
3. Ingrao, C., Lo Giudice, A., Bacenetti, J., Tricase, C., Dotelli, G. et al. (2015). Energy and environmental assessment of industrial hemp for building applications: a review. *Renewable & Sustainable Energy Reviews, 51,* 29-42.

4. Fangueiro, R., Rana S. (2016). *Natural fibres: advances in science and technology towards industrial applications*, RILEM book series 12. Springer, Netherlands.
5. Maalouf, C., Ingrao, C., Scrucca, F., Moussa, T., Bourdot, A. et al. (2018). An energy and carbon footprint assessment upon the usage of hemplime concrete and recycled-PET façades for office facilities in France and Italy. *Journal of Cleaner Production, 170,* 1640-1653.
6. Hetemäki, L., Hanewinkel, M., Muys, B., Ollikainen, M., Palahí, M. et al. (2017). *Leading the way to a European circular bioeconomy strategy. From Science to Policy* 5. European Forest Institute. http://www2.efi.int/files/attachments/publications/efi_fstp_5_2017.pdf.
7. Das, S. (2017). Mechanical and water swelling properties of waste paper reinforced unsaturated polyester composites. *Construction and Building Materials,* 138*,* 469-478.
8. Soydan, A. M., Sari, A. K., Duymaz, B., Akdeniz, R., Tunaboylu, B. (2018). Air-cured fiber-cement composite mixtures with different types of cellulose fibers. In: Yoo, D. Y., Banthia, N., Fujikake, K., Kim, Y. H., Gupta, R. (eds.), *Advances in materials science and engineering. Special issue: fiber-reinforced cement composites: mechanical properties and structural implications*.
9. Jawaid, M., Md Tahir, P., Saba, N. (2017). *Lignocellulosic fibre and biomass-based composite materials*, 1st ed. Woodhead Publishing.
10. Célino, A., Fréour, S., Jacquemin, F., Casari, P. (2013). The hygroscopic behavior of plant fibers: a review. *Frontiers in Chemistry, 1.*
11. Chen, J. Y., Sun, L., Negulescu, I. I., Xu, B. (2017). Fabrication and evaluation of regenerated cellulose/nanoparticle fibers from lignocellulosic biomass. *Biomass Bioenergy, 101,* 1-8.
12. Dungani, R., Abdul Khalil, H. P. S., Sumardi, I., Suhaya, Y., Sulistiawati, E. et al. (2014). Non-wood renewable materials: properties improvement and its application. In: Hakeem, K., Jawaid, M., Rashid, U. (eds.), *Biomass and Bioenergy*, pp. 1-29.
13. Kiruthika, A. V. (2017). A review on physico-mechanical properties of bast fibre reinforced polymer composites. *Journal of Building Engineering, 9,* 91-99.
14. Tabet, T. A., Aziz, F. A. (2013). Cellulose microfibril angle in wood and its dynamic mechanical significance. In: Van De Ven, T. G. M. (ed.), *Cellulose-fundamental aspects*, pp. 113-142. London: IntechOpen.
15. Neto, A. R. S., Araujo, M. A. M., Barboz, R. M. P., Fonseca, A. S., Tonoli, G. H. D. et al. (2015). Comparative study of 12 pineapple leaf fiber varieties for use as mechanical reinforcement in polymer composites. *Industrial Crops and Products, 64,* 68-78.
16. Neagu, R. C., Gamstedt, E. K., Berthold, F. (2006). Stiffness contribution of various wood fibers to composite materials. *Journal of Composite Materials, 40,* 663-699.
17. Mobasher, B. (2012). *Mechanics of fiber and textile reinforced cement composites*, pp. 352. Boca Raton, London, New Yourk: CRC Press, Taylor & Francis Group.
18. Roma Jr., L. C., Luciane, S. M., Savastano Jr., H. (2008). Evaluation of mechanical, physical and thermal performance of cement-based tiles reinforced with vegetable fibers. *Construction and Building Materials, 22,* 668-674.
19. Tonoli, G. H. T., Rodrigues Filho, U. P., Savastano Jr., H., Bras, J., Belgacem, M. N. et al. (2009). Cellulose modified fibres in cement based composites. *Composites: Part A, 40,* 2046-2053.
20. Ashori, A., Tabarsa, T., Valizadeh, I. (2011). Fiber reinforced cement boards made from recycled newsprint paper. *Materials Science and Engineering A, 528,* 7801-7804.
21. Stevulova, N., Cigasova, J., Estokova, A., Terpakova, E., Geffert, A. et al. (2014). Properties characterization of chemically modified hemp hurds. *Materials, 7,* 8131-8150.
22. Kacik, F., Kacikova, D., Jablonsky, M., Katuscak, S. (2009). Cellulose degradation in new-sprint paper ageing. *Polymer Degradation and Stability, 94,* 1509-1514.
23. Segal, L., Creely, J. J., Martin, A. E., Conrad, C. M. (1962). An empirical method for estimating the degree of crystallinity of native cellulose using the X-ray diffractometer. *Textile Research Journal, 29(10),* 786-794.
24. Dai, D., Fan, M. (2010). Characteristic and performance of elementary hemp fibre. *Materials Sciences and Applications, 1,* 336-342.
25. Poletto, M., Ornaghi, H. L., Zattera, A. J. (2014). Native cellulose: structure, characterization and thermal

properties. *Materials, 7,* 6105-6119.

26. STN EN 196-1. Methods of testing cement. Part 1: Determination of strength. Bratislava (Slovakia): Office of Standards, Metrology and Testing. 2016.
27. STN EN 1015-11/A1. Methods of testing mortars for masonry. Part 11: Determination of flexural and compressive strength of hardened mortar. Bratislava (Slovakia): Office of Standards, Metrology and Testing. 2007.
28. STN EN 1015-18. Methods of testing mortars for masonry. Part 18: Determination of the capillary water absorption coefficient of hardened mortar. Bratislava (Slovakia): Office of Standards, Metrology and Testing. 2003.
29. Campano, C., Miranda, R., Merayo, N., Negro, C., Blanco, A. (2017). Direct production of cellulose nanocrystals from old newspapers and recycled newsprints. *Carbohydrate Polymers, 173,* 489-496.
30. Mwaikambo, L. Y., Ansell, M. P. (2001). The determination of porosity and cellulose content of plant fibers by density methods. *Journal of Materials Science Letters, 20,* 2095-2096.
31. Razali, N., Salit, M. S., Jawaid, M., Ishak, M. R., Lazim, Y. (2015). A study on chemical composition, physical, tensile, morphological, and thermal properties of roselle fibre: Effect of fiber maturity. *BioResources, 10,* 1803-1823.
32. Thommes, M., Kaneko, K., Neimark, A. V., Olivier, J. P., Rodriguez-Reinoso, F. et al. (2015). Physisorption of gases with special reference to the evaluation of surface area and pore size distribution (IUPAC Technical Report). *Pure Applied Chemistry, 87,* 1051-1069.
33. Chen, Y., Wang, Y., Wan, J., Ma, Y. (2010). Crystal and pore structure of wheat straw cellulose fiber during recycling. *Cellulose, 17,* 329-338.
34. Daniel, T. (2002). Changes of cellulose fiber wall structure during drying investigated using NMR self diffusion and relaxation experiments. *Cellulose, 9,* 139-147.
35. Xu, Q. H., Gao, Y., Qin, M. H., Wu, K. L., Fu, Y. J. et al. (2013). Nanocrystalline cellulose from aspen kraft pulp and its application in deinked pulp. *International Journal of Biological Macromolecules, 60,* 241-247.
36. Hon, D. N. S. (1994). Cellulose, a random-walk along its historical path. *Cellulose, 1,* 1-25.
37. Rodriguez-Blanco, J. D., Shaw, S., Benning, L. G. (2011). The kinetics and mechanisms of amorphous calcium carbonate (ACC) crystallization to calcite, via vaterite. *Nanoscale, 3,* 265-271.
38. Reyes, C. A. R., Williams, C., Alarcón, O. M. C. (2013). Nucleation and growth process of sodalite and cancrinite from kaolinite-rich clay under low-temperature hydrothermal conditions. *Materials Research, 16,* 424-438.
39. Lu, P., Hsieh, Y. L. (2012). Preparation and characterization of cellulose nanocrystals from rice straw. *Carbohydrate Polymers, 87,* 564-573.
40. Correia, V. C., dos Santos, V., Sain, M., Santos, S. F., Leão, A. L. et al. (2016). Grinding process for the production of nanofibrillated cellulose based on unbleached and bleached bamboo organosolv pulp. *Cellulose, 23,* 2971-2987.
41. Sjöholm, E. (2004). Size exclusion chromatography of cellulose and cellulose derivatives. In: Wu, C. (ed.), *Handbook of size exclusion chromatography and related techniques*, 2nd ed, pp. 1-44. Marcel Dekker Inc.
42. Zimmermann, T., Bordeanu, N., Strub, E. (2010). Properties of nanofibrillated cellulose from different raw materials and its reinforcement potential. *Carbohydrate Polymers, 79,* 1086-1093.
43. Khai, D. M., Nhan, P. D., Hoanh, T. D. (2017). Average molecular weight and molecular weight distribution of the Vietnamese acacia pulps. *Vietnam Journal of Chemistry, 55,* 135-138.
44. Oberlerchner, J. T., Rosenau, T., Potthast, A. (2015). Overview of methods for the direct molar mass determination of cellulose. *Molecules, 20,* 10313-10341.
45. Xu, F., Yu, J., Tesso, T., Dowell, F., Wang, D. (2013). Qualitative and quantitative analysis of lignocellulosic biomass using infrared techniques: a mini-review. *Applied Energy, 104,* 801-809.
46. Popescu, M. C., Popescu, C. M., Lisa, G., Sakata, Z. (2011). Evaluation of morphological and chemical aspects of different wood species by spectroscopy and thermal methods. *Journal of Molecular Structure, 988,* 65-72.
47. Rosa, R. M. F., Medeiros, E. S., Malmonge, J. A., Gregorski, K. S., Wood, D. F. et al. (2010). Cellulose nanowhiskers from coconut husk fibers: Effect of preparation conditions on their thermal and morphological behaviour. *Carbohydrate Polymers, 81,* 83-92.
48. Fackler, K., Stevanic, J. S., Ters, T., Hinterstoisser, B., Schwanninger, M. et al. (2011). FT-IR imaging

spectroscopy to localise and characterise simultaneous and selective white-rot decay within sprude wood cell. *Holzforschung, 65,* 411-420.

49. Saikia, B. J., Parthasarathy, G. (2010). Fourier transform infrared spectroscopic characterization of kaolinite from Assam and Meghalaya, Northeastern India. *Journal of Modern Physics, 1,* 206-210.
50. Rong, X., Huang, Q., He, X., Chen, H., Cai, P. et al. (2008). Interaction of Pseudomonas putida with kaolinite and montmorillonite: a combination study by equilibrium adsorption, ITC, SEM and FTIR. *Colloids and Surfaces B, 64,* 49-55.
51. Zuraida, A., Norshahida, S., Sopyan, I., Zahurin, H. (2011). Effect of fiber length variations on properties of coir fiber reinforced cement-albumen composite (CFRCC). *IIUM Engineering Journal, 12,* 63-76.
52. Stevulova, N., Estokova, A., Cigasova, J., Schwarzova, I., Kacik, F. et al. (2017). Thermal degradation of natural and treated hemp hurds under air and nitrogen atmosphere. *Journal of Thermal Analysis and Calorimetry, 128,* 1649-1660.
53. Hoi, L. W. S., Martincigh, B. S. (2013). Sugar cane plant fibres: Separation and characterisation. *Industrial Crops and Production, 47,* 1-12.
54. Nakamura, K., Hatakeyma, T., Hatakeyama, H. (1981). Studies of bound water of cellulose by differential scanning calorimetry. *Textile Research Jounal, 51,* 607-613.
55. Gomes, L. M., Aroche, A., Schafer, M., Erhart, R., Moraes, C. A. M. et al. (2015). Influence of cellulose pulp waste in plastering mortar. *Key Engineering Materials, 634,* 222-234.
56. Jonoobi, M., Niska, K. O., Harun, J., Misra, M. (2009). Chemical composition, crystallinity, and thermal degradation of bleached and unbleached kenaf bast (Hibiscus cannabinus) pulp and nanofibers. *BioResources, 4,* 626-639.
57. Kim, H. S., Kim, S., Kim, H. J., Yang, H. S. (2006). Thermal properties of bio-flour-filled polyolefin composites with different compatibilizing agent type and content. *Thermochimica Acta, 451,* 181-188.
58. Kabir, M. M., Wang, H., Lau, K. T., Cardona, F. (2013). Effects of chemical treatments on hemp fibre structure. *Applied Surface Science, 276,* 13-23.
59. Alemdar, A., Sain, M. (2008). Biocomposites from wheat straw nanofibers: morphology, thermal and mechanical properties. *Composites Science and Technology, 68,* 557-565.
60. Poletto, M., Zattera, A. J., Forte, M. M., Santana, R. M. (2012). Thermal decomposition of wood: Influence of wood components and cellulose crystallite size. *Bioresource Technology, 109,* 148-153.
61. Dweck, J. (2008). Qualitative and quantitative characterization of Brazilian natural and organophilic clays by thermal analysis. *Journal of Thermal Analysis and Calorimetry, 92,* 129-135.
62. Trusilewicz, L. N., Fernandez Martinez, F., Rahhal, V., Talero Morales, R. (2012). TEM and SAED characterization of metakaolin. Pozzolanic activity. *Journal of American Ceramic Society, 95,* 2989-2996.
63. Tian, M., Qu, I., Zhang, X., Zhang, K., Zhu, S. et al. (2014). Enhanced mechanical and thermal properties of regenerated cellulose/grapheme composite fibers. *Carbohydrate Polymers, 111,* 456-462.
64. Sombatsompop, N., Wood, A. K. (1997). Measurement of thermal conductivity of polymers using an improved lee's disc apparatus. *Polymer Testing, 16,* 203-223.